Ru-promoted perovskites as effective redox catalysts for CO_2 splitting and methane partial oxidation in a cyclic redox scheme

Sherafghan Iftikhar[1], William Martin[1], Xijun Wang[1], Junchen Liu[1], Yunfei Gao[1,2], and Fanxing Li[1]*

[1] Department of Chemical and Biomolecular Engineering, North Carolina State University, Raleigh, NC 27695-7905, United States

[2]Key Laboratory of Coal Gasification and Energy Chemical Engineering of Ministry of Education, Shanghai Engineering Research Center of Coal Gasification, East China University of Science and Technology, Shanghai 200237, PR China

*fli5@ncsu.edu

This file includes:

- Supplementary text
- Fig. S1: DTG profiles of (a) LFM during CH_4-TPR, (b) Ru-LFM during CH_4-TPR, (c) LFM during CO_2-TPO, (d) Ru-LFM during CO_2-TPO, (e) LFM during H_2-TPR, and (f) Ru-LFM during H_2-TPR.
- Fig. S2: Fitting chart of the weight loss peaks for TPR/TPO experiments in Fig. S1 (R^2 ~ 0.85-0.99).
- Fig. S3: XRD spectra of LFM and Ru-impregnated LFM samples.
- Fig. S4: Weight loss/gain during CH_4 -TPR and CO_2 -TPO of Ru-LFM sample
- Fig. S5: H_2 / CO ratio during 120 cycles over Ru-LFM.
- Fig. S6: EDS mapping of fresh, post-100 cycles, and post-O_2 TPO Ru-LFM samples.

Supplementary text:

Definitions of conversions and selectivity:

$$CH_4\ Conversion\ = 100 \times \frac{CH_{4,in} - CH_{4,out}}{CH_{4,in}}$$

$$CO\ Selectivity\ = 100 \times \frac{CO_{out}}{CO_{out} + CO_{2,out}}$$

$$CO_2\ Conversion\ =\ 100\ x\ \frac{CO_{2,in} - CO_{2,out}}{CO_{2,in}}$$

Thermodynamics analysis of methane POx and CO_2-Splitting reactions: The dotted black lines in the Ellingham diagram (Fig.2) correspond to the variation of ΔG with the temperature at a given P_{O_2} and these lines were drawn by using the following equation:

$$\Delta G\ =\ -\ RT \ln P_{O_2} \qquad \text{(E1)}$$

Theoretical CO_2 conversion was calculated using the following set of equations:

$$2CO_2 \leftrightharpoons 2CO + O_2 \qquad \text{(E2)}$$

$$K = \frac{P_{O_2}}{P_o}\left(\frac{P_{CO}}{P_{CO_2}}\right)^2 \qquad \text{(E3)}$$

$$CO_2\ Conversion\ =\ 100\ x\ \frac{P_{CO}}{P_{CO_2} + P_{CO}} \qquad \text{(E4)}$$

$$CO_2\ Conversion\ =\ 100\ x\ \frac{\frac{P_{CO}}{P_{CO_2}}}{1 + \frac{P_{CO}}{P_{CO_2}}} \qquad \text{(E5)}$$

$$CO_2\ Conversion\ =\ 100\ x\ \frac{\sqrt{K}}{\sqrt{K} + \sqrt{\frac{P_{O_2}}{P_o}}} \qquad \text{(E6)}$$

Calculation of Gibbs free energy change (ΔG)

Gibbs free energy change (ΔG) can be related to P_{O_2} (or oxygen chemical potential, u_{O_2}) within specified δ ranges. $A_xA'_{1-x}B_yB'_{1-y}O_{3-\delta}$ oxygen carriers' redox thermodynamics can be described by their incremental Gibbs free energy as $\Delta G_{\delta 1 \rightarrow \delta 2} = \Delta G_{\delta 2} - \Delta G_{\delta 1+}\left(\frac{\delta 2 - \delta 1}{2}\right)u_{O_2}$, where $\delta 1 \rightarrow \delta 2$ represent the

change of δ value from $\delta 1$ to $\delta 2$. The slope of the δ vs. G curve thus describe the u_{O_2} within a vacancy concentration range at a given temperature. They can in turn be used to determine the feasibility and capacity of oxygen uptake and release within a given P_{O_2} and/ or temperature swings. As one can anticipate, too large or too small $\Delta G_{\delta 1 \rightarrow \delta 2}$ will lead to less or over stable configurations. Therefore, a suitable as $\Delta G_{\delta 1 \rightarrow \delta 2}$ within an optimal range over a large δ span would lead to a larger oxygen capacity. Previous experiments indicate that δ usually varies in the range of 0.25– 0.5 in chemical processes. It is also noted that every 0.125 change in δ correspond to roughly 1 wt% oxygen capacity.

Calculation of activations energies

Activation energies for the CH_4-POx and CO_2 splitting reactions were calculated using the Kissinger method:

$$\ln\left(\gamma T_o^{-2}\right) = -E_a(RT_o)^{-1} + \ln\left(AR\,E_a^{-1}\right)$$

Where γ, T_p, A, R and E_a represents the heating rate (°K/min), peak temperature (K), pre-exponential factor, general gas constant(J/mol.K), and the activation energy (kJ/mol), respectively. Various heating rates and peak temperatures from the Fig. S3 were fitted to determine the activation energies as indicated in the Fig. S4.

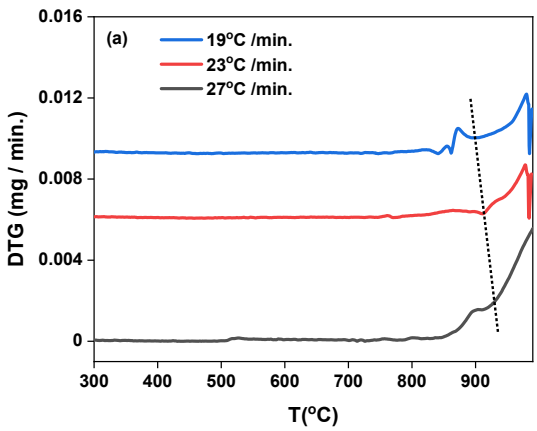

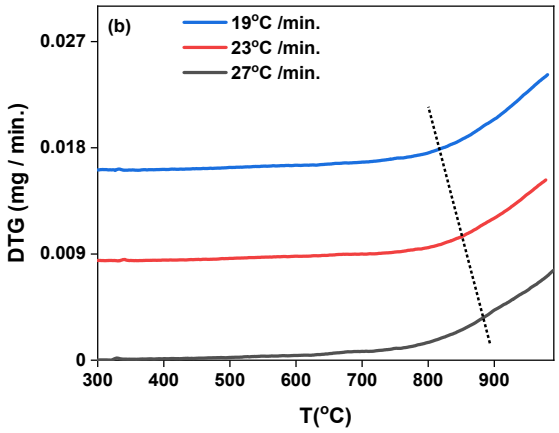

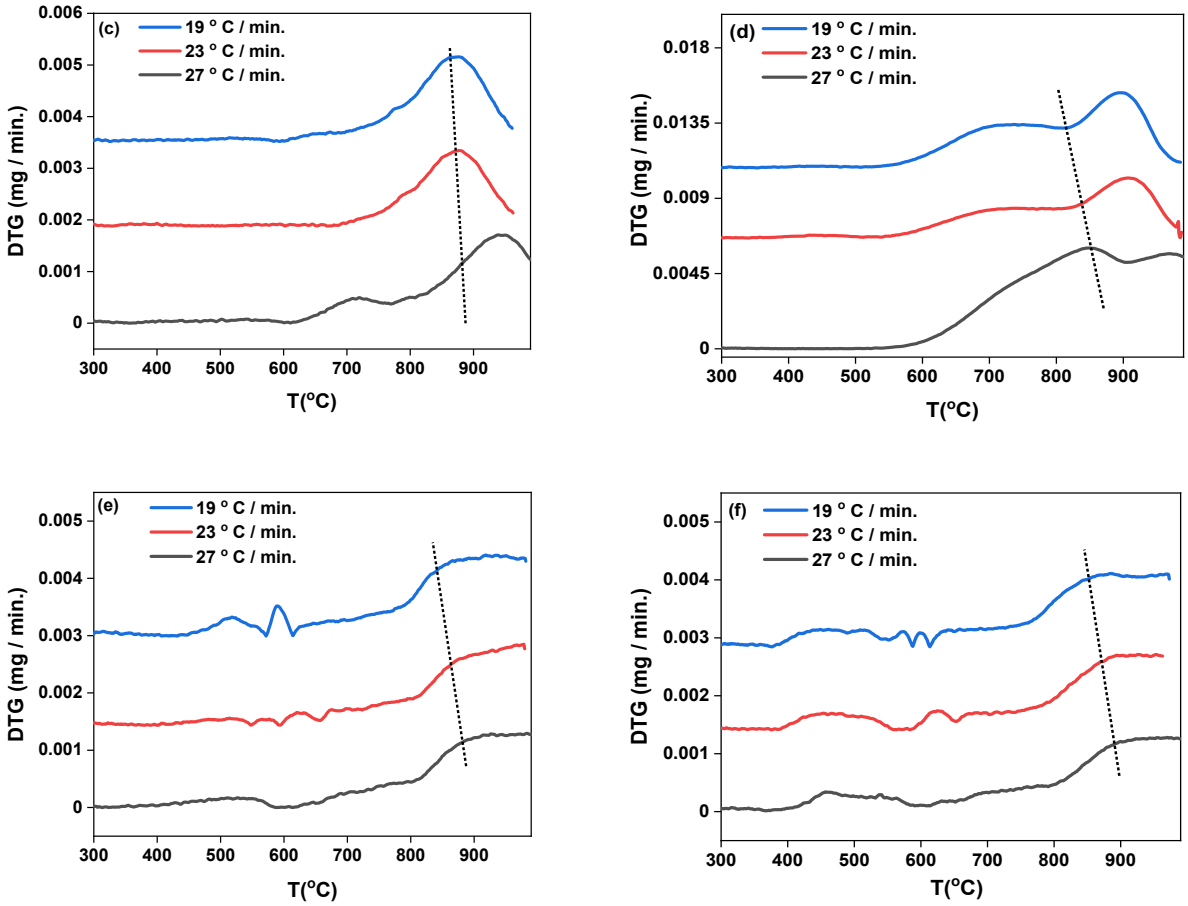

Fig. S1: DTG profiles of (a) LFM during CH_4-TPR, (b) Ru-LFM during CH_4-TPR, (c) LFM during CO_2-TPO, (d) Ru-LFM during CO_2-TPO, (e) LFM during H_2-TPR, and (f) Ru-LFM during H_2-TPR.

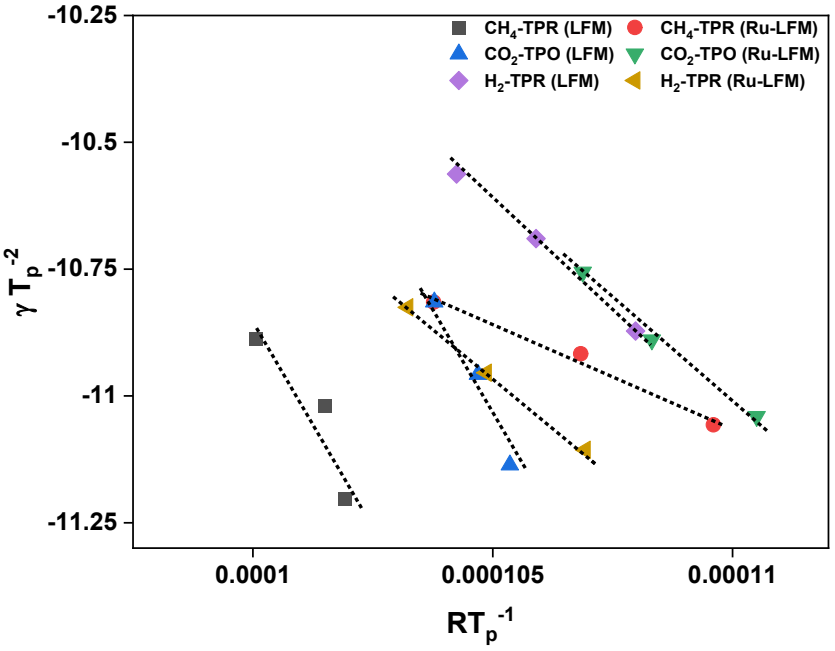

Fig. S2: Fitting chart of the weight loss peaks for TPR/TPO experiments in Fig. S3

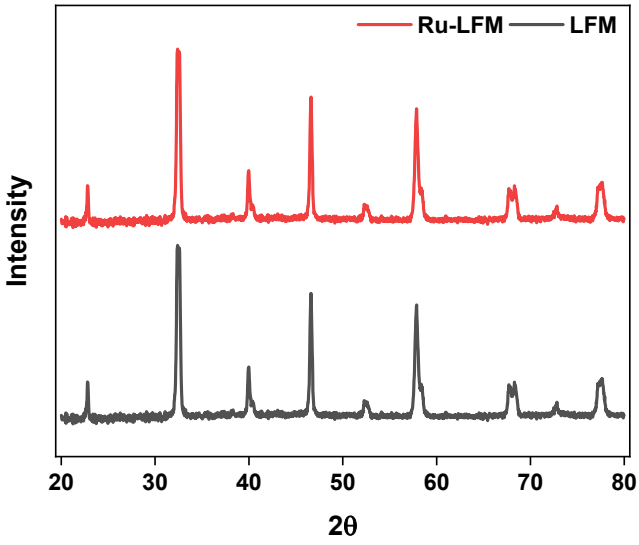

Fig. S3: XRD spectra of LFM and Ru impregnated LFM samples.

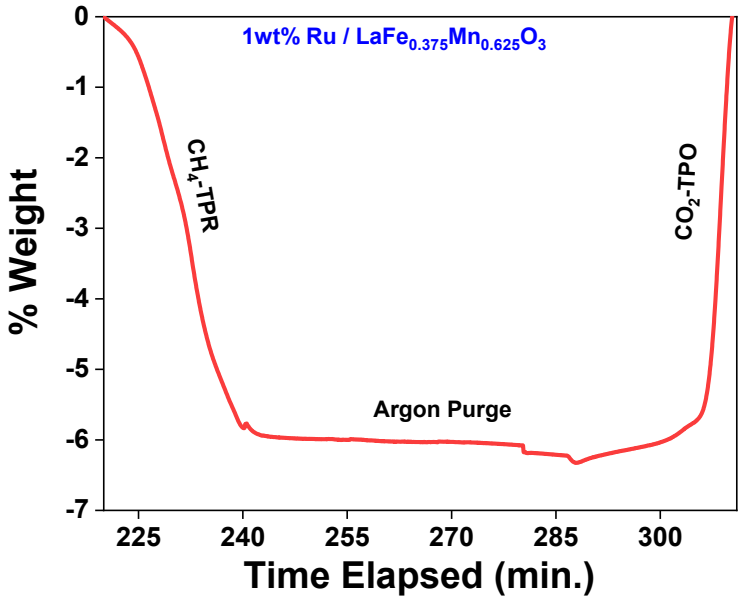

Fig. S4: Weight loss/gain during CH_4 -TPR and CO_2 -TPO of Ru-LFM sample.

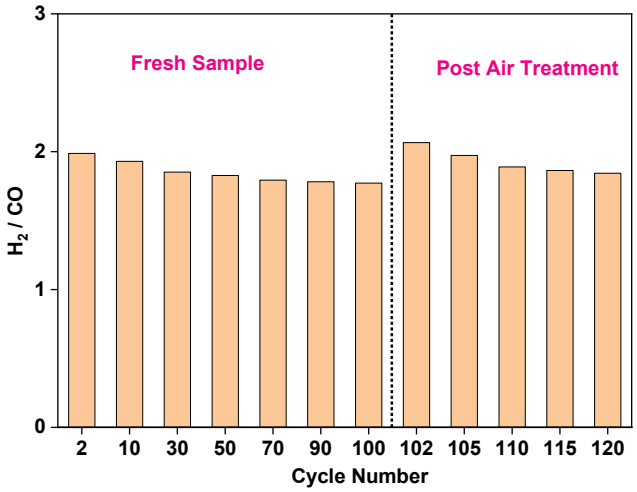

Fig. S5: H_2 / CO ratio during 120 cycles over Ru-LFM

Fresh Ru-LFM **Post-100 Cycles Ru-LFM** **Post O_2-TPO Ru-LFM**

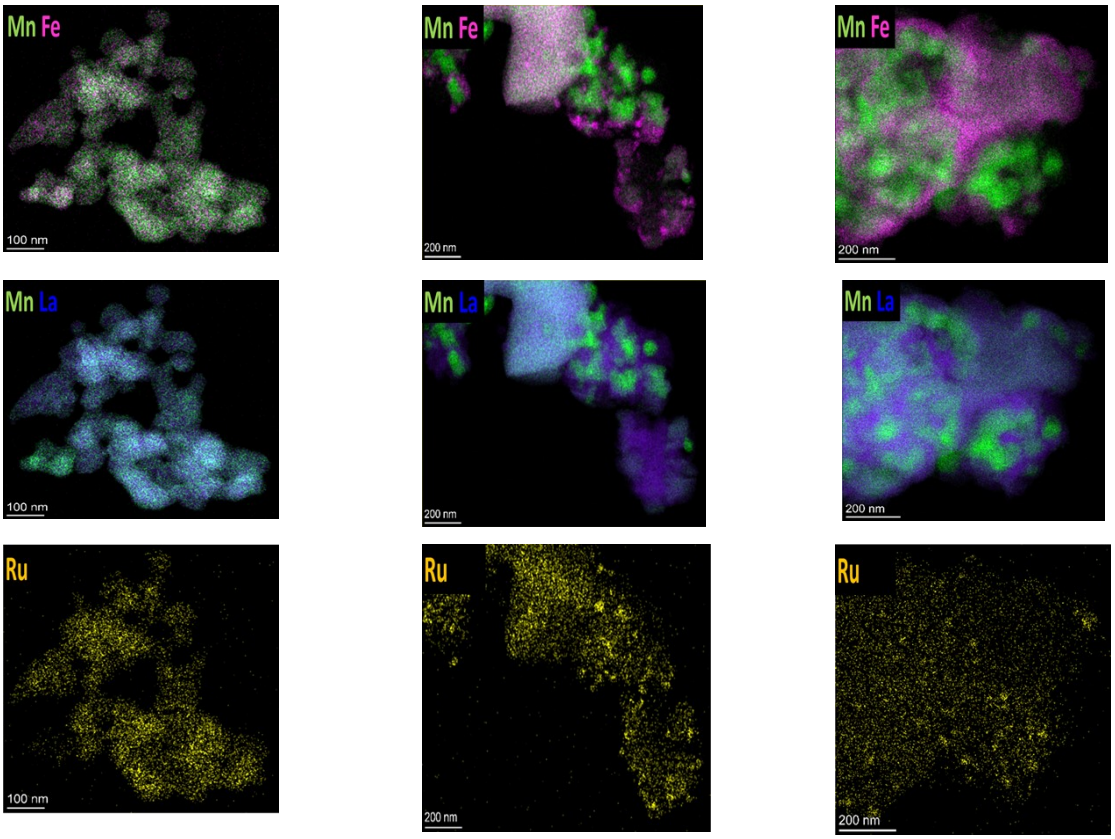

Fig. S6: EDS mapping of fresh, post-100 cycles, and post-O_2 TPO Ru-LFM samples.